Phase detection to measure rotational direction of resonant MEMS mirror driven by parametric excitation

Sangtak Park[1,a], Matthew Wakelin[a], Daniel Malea[a]
[a]Google Canada, 24 Charles St. West, Kitchener, Ontario, N2G 1H2, Canada

ABSTRACT

This paper introduces a new method of detecting the rotational direction of an electrostatic, resonant MEMS mirror with in-plane comb (angular vertical comb) fingers driven by parametric excitation, in which its rotational direction strongly depends on its initial condition due to the nature of its actuation method. In AR applications, this ambiguity on its rotational direction could cause a projected image to be flipped in its scanning direction. To avoid this ambiguity, its rotational direction has to be determined before image projection. To do that, its motion-induced current is measured with a transimpedance amplifier (TIA), and the phase of the motion-induced current at its resonance, f_0, is determined through quadrature demodulation, while the resonant MEMS mirror is driven at twice its torsional resonance, $2f_0$, through parametric excitation. We also validate this concept of phase measurement through a series of experiments with a Laser Doppler Vibrometer (LDV) that optically measures its rotational direction and is used as a reference, as well as a Lock-In Amplifier (LIA) that electrically measures the phase of its motion-induced current at its resonance, f_0, with respect to the optical reference signal from LDV.

Keywords: Resonant MEMS mirror, Parametric excitation, Ambiguity on rotational direction, Phase detection, Motion-induced current, Quadrature demodulation, Laser Beam Scanning (LBS), AR glasses

1. INTRODUCTION

Scanning MEMS mirrors or galvanometers have been extensively used in automotive, commercial, medical, and industrial applications, such as LiDAR[1,10] (Light Detection And Ranging), a pico projector[2,9,22], NED[3,9,20,21] (Near Eye Display) for AR glasses, eye tracking[4], OCR[5] (Optical Coherence Tomography), and Two-photon microscopy[6] and 3D printing based on 2PP[7] (Two Photon Polymerization) or DLW[7] (Direct Laser Writing), to name a few, and most of the scanning MEMS mirrors are made of either a single dual-axis MEMS mirror[8,9,10,22] or two single-axis MEMS mirrors[9,10,22] in Fig. 1. They are also fabricated with different technologies[9,10,22] and operating within different physics[9,10,22]. Most popular types are, for example, electromagnetic[9,10], electrostatic[8,9,10], piezoelectric[9,10], and electrothermal[11,12]. Most MEMS transducers, except for electrostatic MEMS, have a piezoresistive or piezoelectric sensor[9,10] on their supporting structure to measure their bending or angular displacement, while most electrostatic MEMS transducers utilize sensing methods based on change in their capacitance, such as motion-induced current[13] or capacitive sensing[9,10] in general. The maximum opening angle of the resonant MEMS mirror studied in this paper is determined by measuring and converting its motion-induced current to voltage with TIA.

This research focuses on an electrostatically-actuated, resonant MEMS mirror driven parametrically in AR applications, providing a straightforward and precise solution to the problem of the ambiguity in its scanning direction due to strong dependence on its initial conditions. The first parametric excitation[14] applied to MEMS was reported in 1998. Ever since, parametric excitation[14,15,19,23,24,25] has been widely used in sensing

[1] sangtak@google.com; tel.: 1-519-513-3334 (office); www.google.com

applications due to its high quality factor and high sensitivity to stimuli. In most sensing applications based on MEMS transducers, the phase of MEMS transducers' motion with respect to their excitation signal is not of great interest, but the magnitude of their motion is. However, for the resonant MEMS mirror in AR applications, we need to precisely measure both phase and magnitude of its torsional motion at resonance, because its phase and magnitude correspond to the scanning direction of the raster lines and the opening angle of the resonant MEMS mirror, respectively. In other words, this ambiguity in its rotational direction could cause a projected image to be flipped in its scanning direction. To avoid this ambiguity, its scanning direction has to be determined before image projection.

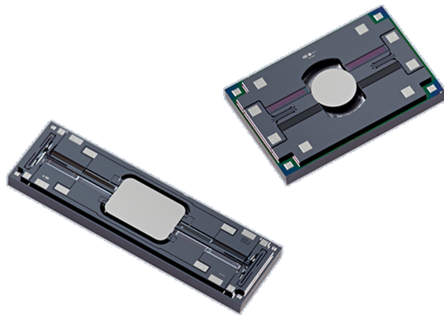

Fig. 1a Optical pictures of electrostatically-actuated, quasi-static (left) and resonant (right) MEMS mirrors fabricated by ST Microelectronics[2,18,19,24,25] (STM) and made of two wafers: A top structural wafer and a bottom handling wafer. (courtesy of STM)

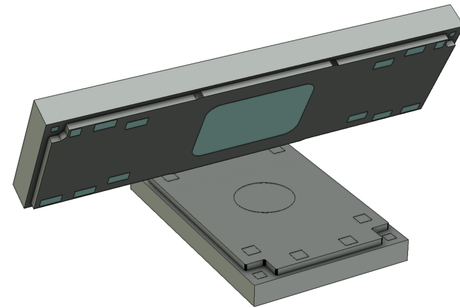

Fig. 1b One opto-mechanical configuration of laser beam scanning (LBS) based on two single-axis MEMS mirrors: the resonant MEMS mirror is located in the bottom and the quasi-static MEMS mirror is positioned in the top.

Although various optical sensing methods exist and could be utilized to measure its scanning direction, these optical sensing methods are not suitable in AR applications due to their big form factor and high power consumption, as well as high cost. Hence, its motion-induced current is measured with TIA, and the phase of the motion-induced current at its torsional resonance, f_0, is determined through quadrature demodulation, while the resonant MEMS mirror is driven at twice its torsional resonance with high-voltage (HV) and slew-rate controlled, actuation signal. Since its resonant motion at f_0 is driven by the HV actuation signal at $2f_0$ via parametric excitation, the current induced by this HV actuation signal does not have any frequency component at its resonance, f_0. In addition, the most current induced by its resonant motion is also located at twice its resonance, $2f_0$, due to its geometric symmetry in Fig. 2. In other words, its torsional (mechanical) motion at resonance causes capacitive changes at twice its mechanical resonance due to the geometric symmetry. However, there is a small difference in their capacitance due to fabrication uncertainties or intentional designs. This disparity introduces very small motion-induced current at its mechanical resonance, and its phase solely depends on its scanning direction due to this geometric asymmetry. We successfully demonstrate this newly proposed method to detect the rotational direction of the resonant MEMS mirror by measuring the phase of the motion-induced current at f_0 with quadrature demodulation. It is also independently confirmed with LDV (Polytec), while its motion-induced current is measured with TIA and quadrature-demodulated by LIA (Zurich Instruments).

2. RESONANT MEMS MIRROR

As mentioned, the raster scanning could be achieved by a pair of two single-axis MEMS mirrors; The resonant MEMS mirror generates two raster scan lines per period, while the quasi-static MEMS mirror rotates

at a frame rate, much lower than its resonance, in an orthogonal direction to the scanning direction of the resonant MEMS mirror that operates at its torsional resonance ranging from 20 kHz to 30 kHz, away from human audible spectrum. The optical image of the resonant MEMS mirror with in-plane comb fingers driven by parametric excitation is presented in Fig. 2. Since its comb fingers are in-plane, a single structural layer[2] is used to fabricate every functional structure, such as a mirror plate, torsion bars, and comb fingers.

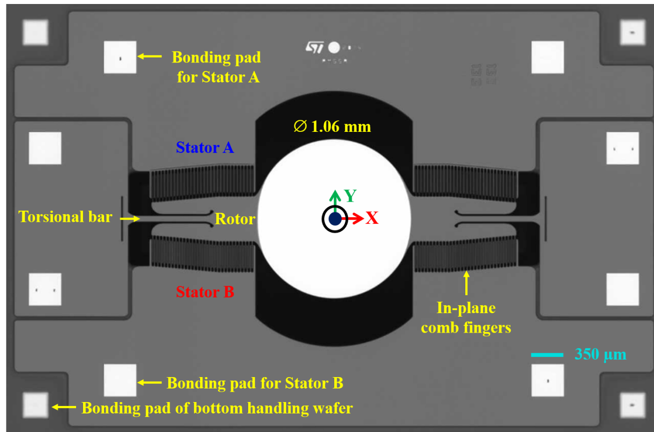

Fig. 2 Top view of the electrostatic, resonant MEMS mirror driven by parametric excitation, which is fabricated by STM: The in-plane comb (AVC, angular vertical comb[16,19,25]) fingers are located on both its rotors and stators without any depth difference in the Z axis; Its mirror plate is 1.06 mm in diameter and structurally supported by two torsion bars; All of its functional structures are fabricated on the top wafer, while its bottom wafer is used for handling.

The simplified circuit diagram showing electrical connections for sensing and actuation of the resonant MEMS mirror is presented in Fig. 3, where two stators are electrically connected together and DC-biased at -20 V, while the HV actuation signal is applied to the rotor of the resonant MEMS mirror. The back-to-back diodes (D1) and the AC-coupling capacitor (C_{in}) to the inverting input of TIA (U1) in Fig. 3 act as a bias tee providing separation between the DC and AC paths: the DC path for the negative DC bias voltage and the AC path for the motion-induced current of the resonant MEMS mirror.

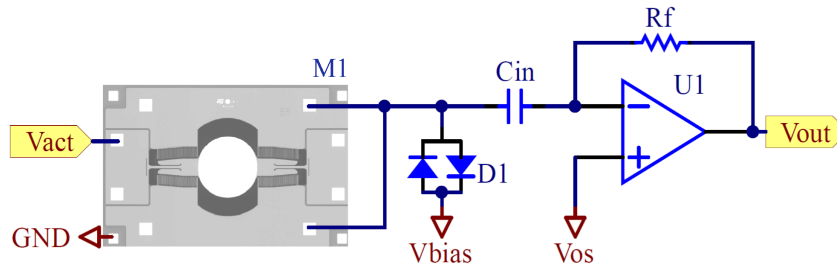

Fig. 3 Simplified circuit diagram showing the electrical connections to the resonant MEMS mirror (M1) for its sensing and actuation: Vact, Vbias, Vos, and Vout represent the HV actuation (excitation) voltage applied to its rotor, the negative DC bias voltage applied to both stators, the DC offset voltage of TIA (U1), and the output voltage of TIA (U1), respectively.

Since both stators of the resonant MEMS mirror are electrically connected together to the same node shown in Fig. 3, its MEMS capacitance between its rotor and stators could be expressed as a single function of its mechanical angle in degree, as presented in Fig. 4a. The capacitance of the resonant MEMS mirror is the biggest at rest or zero angle, because it has in-plane comb fingers (AVC[16,19]), not staggered vertical comb (SVC[16]) fingers used in the quasi-static MEMS mirror. The partial derivative of the MEMS capacitance with respect to its torsional angle is also presented in Fig. 4b, and its motion-induced current is presented in Eq. 1.

$$i(t) = \frac{dC_m(\theta)}{d\theta}\frac{d\theta}{dt}V(t) + \left(C_p + C_m(\theta)\right)\frac{dV(t)}{dt} \quad (1)$$

where, i, C_m, Θ, V, and C_p represent the total current induced by the HV actuation signal and the induced motion, the MEMS capacitance, the mechanical, torsional angle, the potential difference between its rotor and stators, and the parasitic capacitance considered as constant, respectively.

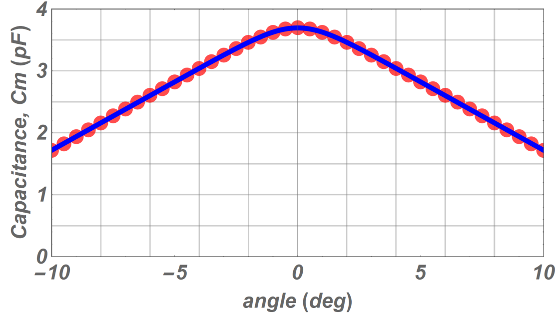

Fig. 4a Capacitance of the resonant MEMS mirror depending on its torsional angle: The red circles and blue solid line represent its capacitance obtained from FEM at discrete angles and interpolation, respectively.

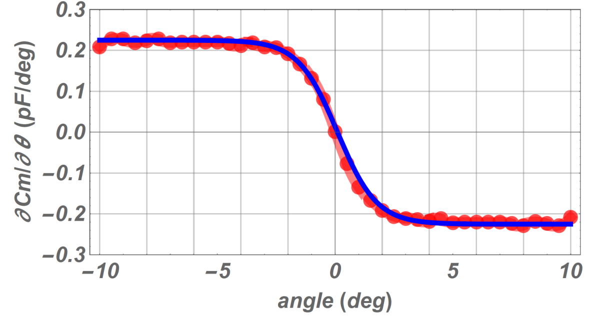

Fig. 4b Partial derivative of MEMS capacitance with respect to its torsional angle: the red circles and blue solid line represent its partial derivative of capacitance and the nonlinear fit based on a sigmoid function, respectively.

The first term in the right side of Eq. 1 represents the motion-induced current of the resonant MEMS mirror, and the second term in Eq. 1 represents the current induced by the HV actuation signal. In general, the voltage-induced current is three orders of magnitude larger than the motion-induced current, causing the saturation at the output of TIA, as presented in Fig. 5, assuming the resonant MEMS mirror is driven at twice its resonance. The motion-induced currents measured with TIA at two different (mechanical) opening angles, ±5 and ±10 deg, are presented in Fig. 6a and 6b to show the relationship between the opening angle of the resonant MEMS mirror and the output of TIA.

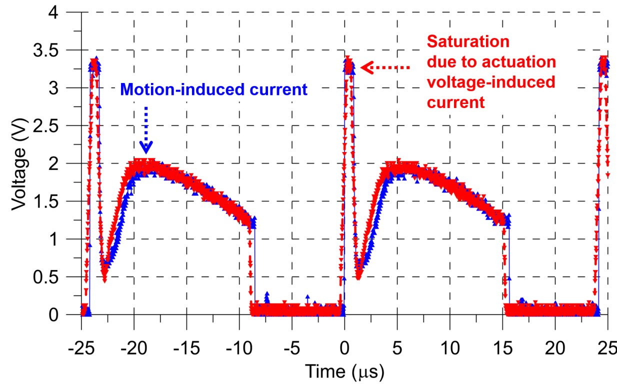

Fig. 5a Output of TIA that measures and amplifies the current induced by both HV actuation signal, 130 V, and the motion of the resonant MEMS mirror driven by parametric excitation at twice its torsional resonance, 41.3 kHz, while it oscillates at its torsional resonance, 20.65 kHz.

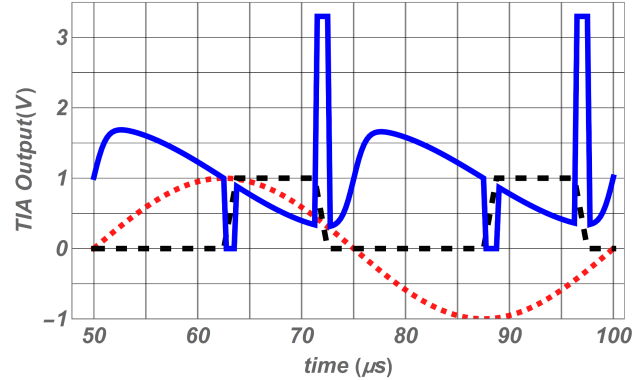

Fig. 5b Normalized angular displacement (red-dotted), normalized & slew-rate controlled HV actuation signal (black-dashed), and the output of TIA with 1 V DC offset voltage (blue-solid); the actual output of TIA is saturated at GND and 3.3 V due to its power rails, and this saturation occurs at both leading and falling edges.

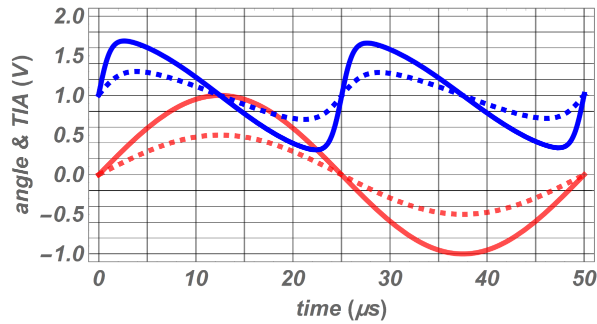

Fig. 6a Normalized ±5° (red-dashed) and ±10° (red-solid) opening angles of the resonant MEMS mirror and corresponding outputs of TIA, ±5° (blue-dashed) and ±10° (blue-solid) without the saturation for clarity.

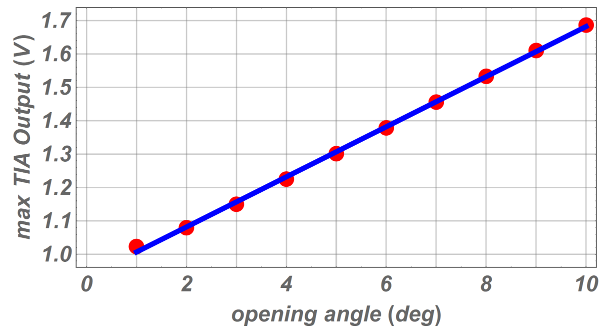

Fig. 6b Max. output voltage of TIA vs peak opening angle of the resonant MEMS mirror from ±1° to ±10°: the red circles and blue line represent max. voltage of TIA obtained by simulation and linear regression, respectively.

3. EXPERIMENTS

Before characterizing the resonant MEMS mirror with LDV, its Finite Element Model (FEM) is created with COMSOL to determine its mode shapes and corresponding frequencies of resonance; its two mode shapes under 100 kHz are identified and presented in Fig. 7. Its operating mode shape is the primary torsional motion at its first resonance, 20.7 kHz, as shown in Fig. 7a and 8a. Its other spurious modes are also determined through FEA and measured with LDV, being presented in Fig. 7b, and Fig. 8b and 8c.

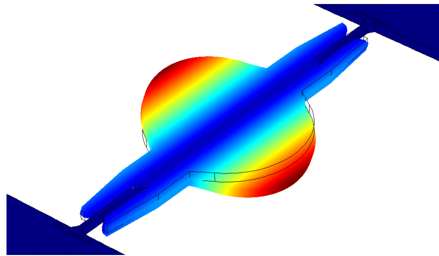

Fig. 7a Primary torsional mode shape of the resonant MEMS mirror at 21 kHz, obtained with COMSOL®

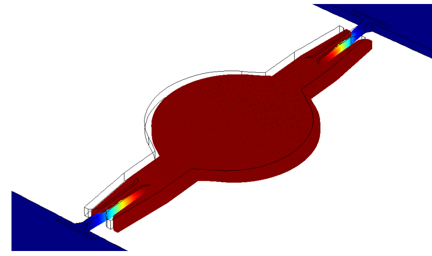

Fig. 7b First spurious mode shape of in-plane bending determined at 28 kHz

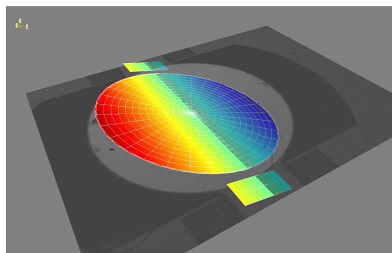

Fig. 8a Primary torsional motion measured at 20.7 kHz with LDV

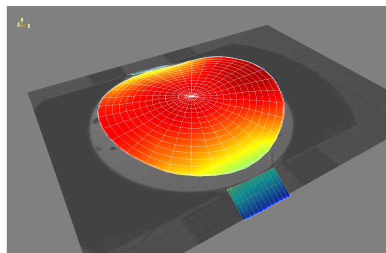

Fig. 8b Out-of-plane bending (piston) motion at 144.7 kHz

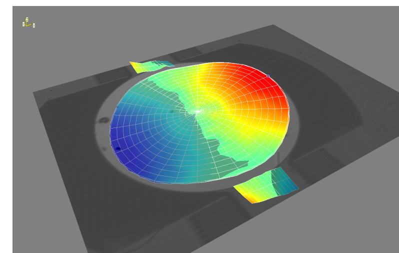

Fig. 8c Twisting motion measured at 268.7 kHz

The torsional motion of the resonant MEMS mirror is triggered and excited by the modulation of its torsional stiffness due to its in-plane bending motion, i.e. the parametric excitation, described by the nonlinear Mathieu equation[18]. The frequency responses of the resonant MEMS mirror in Fig. 9 shows a typical frequency response of nonlinear systems driven parametrically, exhibiting a very narrow operating bandwidth of 85 Hz and a hysteresis between the frequency responses obtained during sweep-up and sweep-down in frequency, while the resonant MEMS mirror is driven by the HV actuation signal at twice its torsional resonance between 41.2 kHz and 41.6 kHz. Unlike quasi-static MEMS mirrors, the resonant MEMS mirror driven parametrically can not be excited or actuated as presented in Fig. 9, when the excitation or actuation frequency is out of its operating bandwidths or regions described by the Arnold tongue[18].

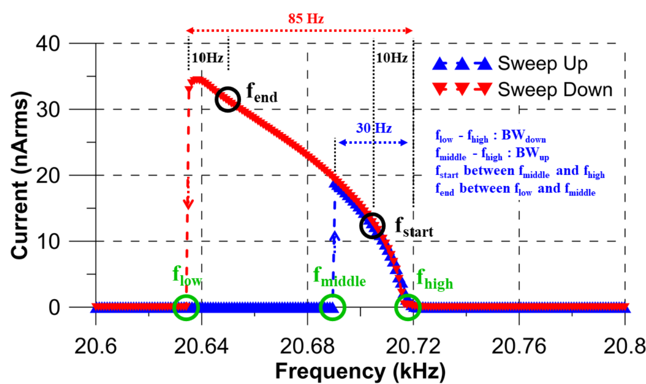

Fig. 9 Frequency responses of the resonant MEMS mirror driven by the HV actuation signal at twice its torsional resonance, $2f_0$, while its current is measured with TIA, and its motion-induced current at its torsional resonance, f_0, is quadrature-demodulated with LIA: the blue and red triangles represent its frequency responses during frequency sweep-up and sweep-down, respectively; A very narrow, asymmetric frequency response is typical of nonlinear systems driven by parametric excitation.

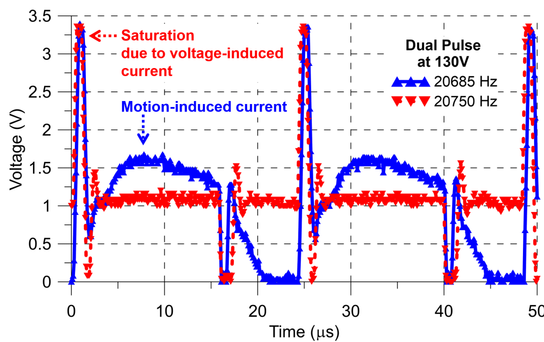

Fig. 10a Outputs of TIA in a time domain: the red-dashed and blue-solid lines represent the induced current without and with the torsional motion, respectively.

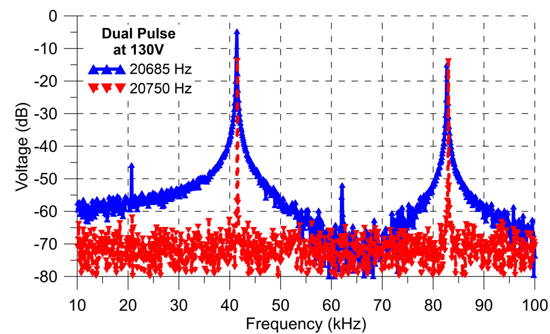

Fig. 10b DFT of the current measured with TIA, while the resonant MEMS mirror is not oscillating (red-dashed) and oscillating at its torsional resonance (blue-solid).

The outputs of TIA captured with an oscilloscope are also shown in Fig. 10a, where the red-dashed line represents the current induced by the HV actuation signal at 41.5 kHz without the torsional motion of the resonant MEMS mirror, while the blue-solid line shows the current induced by both the HV actuation signal at 41.37 kHz, $2f_0$, and its torsional motion at 20.685 kHz, f_0. Although its torsional motion is at 20.685 kHz, half its actuation frequency, the frequency components of its motion-induced current are integer multiples[13] of its fundamental resonance, f_0, as shown in Fig. 10b and Fig. 11. The measured current has two highest magnitudes at $2f_0$ and $4f_0$ caused by the HV actuation signal at $2f_0$ and its harmonics. Hence, it is hard to discern the motion-induced current at $2f_0$ and $4f_0$ from the voltage-induced current at the same frequencies. However, the frequency components of the motion-induced current at f_0 and $3f_0$ are spectrally pure, as

presented in Fig. 10b. i.e. the HV actuation signal does not have these frequency components, and the motion-induced current at f_0 and $3f_0$ only appears with the torsional motion of the resonant MEMS mirror, while not affected by the HV actuation signal. Moreover, we could easily quantify the phase of the torsional motion of the resonant MEMS mirror at f_0 and $3f_0$, as shown in Fig. 11b. Furthermore it turns out that the phase of the motion-induced current at f_0 is very consistent and does not vary much over the entire operating bandwidth, while the phase of the motion-induced current at $3f_0$ varies more than 180 deg.

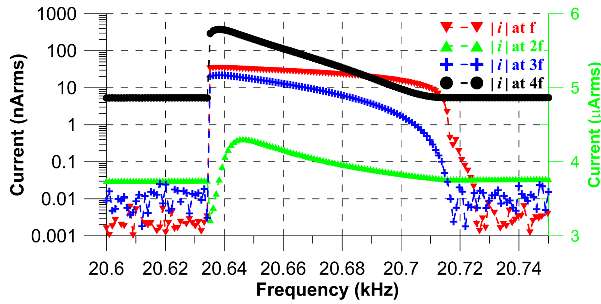

Fig.11a Magnitude of the current measured at each harmonic, while the resonant MEMS mirror is driven parametrically at twice its resonance, 2f.

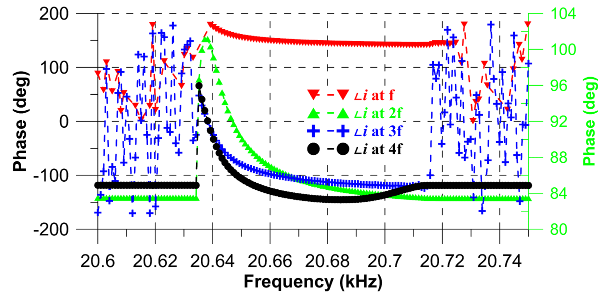

Fig.11b Phases of the current measured with TIA at each harmonic of the torsional motion, such as f, 2f, 3f, and 4f, are demodulated via quadrature demodulation with LIA.

Hence we measure the phase of the motion-induced current at the resonance, f_0, to determine the rotational direction of the resonant MEMS mirror, while it is driven parametrically at twice its resonance, $2f_0$. To validate this new phase detection method, we force the resonant MEMS mirror to rotate either CW or CCW, while using LDV to optically measure its rotation direction, as well as TIA and LIA to measure the phase of the motion-induced current at f_0. The experiment results are presented in Fig. 12b, clearly showing the 180° phase difference between CW (blue) and CCW (red) rotational direction.

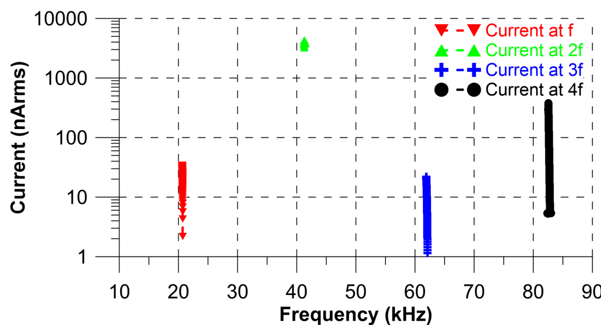

Fig. 12a Frequency components of the motion-induced and the voltage-induced current measured with TIA and demodulated with LIA, while sweeping down the HV actuation frequency from 41.5 kHz to 41.2 kHz.

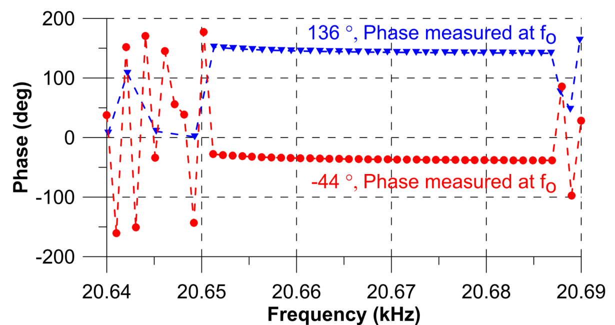

Fig. 12b Two cases of the phase measurement of its motion-induced current at the torsional resonance, f_0, while the resonant MEMS mirror starts to rotate in either CW (blue) or CCW (red) with the HV actuation signal at twice its resonance, $2f_0$.

4. CONCLUSIONS

A resonant MEMS mirror driven parametrically sometimes rotates in an opposite direction due to its strong dependence on initial conditions affected by its orientation, external disturbance, and temperature variation. Although it is not impossible, it is difficult to enforce its rotational direction due to its in-plane comb fingers. Hence, we propose that it would be more robust to measure its rotational direction rather than to enforce it, and we provide the new method to determine its rotational direction, while it is driven by parametric excitation at twice its torsional resonance. Furthermore, we validate this new phase detection method with experiments, where its motion-induced current is measured with TIA, and its rotational direction is determined by the phase of the motion-induced current demodulated with LIA via quadrature demodulation at its torsional resonance. We also show its stable operation due to ample margins between two exclusive rotational directions and the spectral purity of the motion-induced current at torsional resonance.

ACKNOWLEDGEMENT

The authors sincerely appreciate STM's technical support and advice regarding the fabrication of the electrostatic, resonant and quasi-static MEMS mirrors.

REFERENCE

[1] Wang, D., Thomas, L., Koppal, S., Ding, Y. and Xie, H., "A Low-Voltage, Low-Current, Digital-Driven MEMS Mirror for Low-Power LiDAR," IEEE Sens. Lett. 4(8), 1–4 (2020).
[2] Silva, G., Carpignano, F., Guerinoni, F., Costantini, S., De Fazio, M. and Merlo, S., "Optical Detection of the Electromechanical Response of MEMS Micromirrors Designed for Scanning Picoprojectors," IEEE J. Select. Topics Quantum Electron. 21(4), 147–156 (2015).
[3] Kim, M., Lee, S., Jo, Y., Lee, S. and Lee, B., "Compact tomographic near-eye display using a MEMS scanning mirror," Opt. Lett., OL 46(17), 4176–4179 (2021).
[4] Meyer, J., Schlebusch, T., Fuhl, W. and Kasneci, E., "A Novel Camera-Free Eye Tracking Sensor for Augmented Reality Based on Laser Scanning," IEEE Sensors J. 20(24), 15204–15212 (2020).
[5] Chen, Y., Hong, Y.-J., Makita, S. and Yasuno, Y., "Eye-motion-corrected optical coherence tomography angiography using Lissajous scanning," Biomed. Opt. Express, BOE 9(3), 1111–1129 (2018).
[6] Piyawattanametha, W., Cocker, E. D., Burns, L. D., Barretto, R. P. J., Jung, J. C., Ra, H., Solgaard, O. and Schnitzer, M. J., "In vivo brain imaging using a portable 2.9 g two-photon microscope based on a microelectromechanical systems scanning mirror," Opt. Lett., OL 34(15), 2309–2311 (2009).
[7] Pearre, B. W., Michas, C., Tsang, J.-M., Gardner, T. J. and Otchy, T. M., "Fast micron-scale 3D printing with a resonant-scanning two-photon microscope," Additive Manufacturing 30, 100887 (2019).
[8] Drabe, C., Kallweit, D., Dreyhaupt, A., Grahmann, J., Schenk, H. and Davis, W., "Bi-resonant scanning mirror with piezoresistive position sensor for WVGA laser projection systems," presented at SPIE MOEMS-MEMS, 9 February 2012, San Francisco, California, USA, 825209.
[9] Holmstrom, S. T. S., Baran, U. and Urey, H., "MEMS Laser Scanners: A Review," J. Microelectromech. Syst. 23(2), 259–275 (2014).
[10] Wang, D., Watkins, C. and Xie, H., "MEMS Mirrors for LiDAR: A Review," Micromachines 11(5), 456 (2020).
[11] Wang, P., Liu, Y., Wang, D., Liu, H., Liu, W. and Xie, H., "Stability Study of an Electrothermally-Actuated MEMS Mirror with Al/SiO2 Bimorphs," Micromachines 10(10), 693 (2019).

[12] Zhou, L., Yu, X., Feng, P. X.-L., Li, J. and Xie, H., “A MEMS lens scanner based on serpentine electrothermal bimorph actuators for large axial tuning,” Opt. Express, OE 28(16), 23439–23453 (2020).

[13] Park, S., Khater, M., Effa, D., Abdel-Rahman, E. and Yavuz, M., “Detection of cyclic-fold bifurcation in electrostatic MEMS transducers by motion-induced current,” J. Micromech. Microeng. 27(8), 085007 (2017).

[14] Turner, K. L., Miller, S. A., Hartwell, P. G., MacDonald, N. C., Strogatz, S. H. and Adams, S. G., “Five parametric resonances in a microelectromechanical system,” Nature 396(6707), 149–152 (1998).

[15] Li, L., Hiller, T., Bamieh, B. and Turner, K., “Amplitude control of parametric resonances for mass sensing,” IEEE SENSORS 2014 Proceedings, 198–201, IEEE, Valencia, Spain (2014).

[16] Hah, D., Patterson, P. R., Nguyen, H. D., Toshiyoshi, H. and Wu, M. C., “Theory and Experiments of Angular Vertical Comb-Drive Actuators for Scanning Micromirrors,” IEEE J. Select. Topics Quantum Electron. 10(3), 505–513 (2004).

[17] DeMartini, B., Moehlis, J., Turner, K., Rhoads, J., Shaw, S. and Wenhua Zhang., “Modeling of Parametrically Excited Microelectromechanical Oscillator Dynamics with Application to Filtering,” IEEE Sensors, 2005., 345–348, IEEE, Irvine, CA, USA (2005).

[18] Guide, Step, “Laser Beam Scanning,” ST Microelectronics, <https://www.st.com/content/st_com/en/about/innovation---technology/laser-beam-scanning.html> (10 December 2021).

[19] Farrugia, R., Portelli, B., Grech, I., Camilleri, D., Casha, O., Micallef, J. and Gatt, E., “Air damping of high performance resonating micro-mirrors with angular vertical comb-drive actuators,” Microsyst Technol (2019).

[20] Lee, B., Jo, Y., Yoo, D. and Lee, J., “Recent progresses of near-eye display for AR and VR,” Multimodal Sensing and Artificial Intelligence: Technologies and Applications II, S. Negahdaripour, E. Stella, D. Ceglarek, and C. Möller, Eds., 34, SPIE, Online Only, Germany (2021).

[21] Xiong, J., Hsiang, E.-L., He, Z., Zhan, T. and Wu, S.-T., “Augmented reality and virtual reality displays: emerging technologies and future perspectives,” Light Sci Appl 10(1), 216 (2021).

[22] Huikai Xie (Ed.)., [MEMS Mirrors.] (2018).

[23] Ataman, C. and Urey, H., “Modeling and characterization of comb-actuated resonant microscanners,” J. Micromech. Microeng. 16(1), 9–16 (2006).

[24] Frangi, A. A., Guerrieri, A. and Boni, N., “Non-linear dynamics in torsional micromirrors,” 13e colloque national en calcul des structures, Université Paris-Saclay, Giens, Var, France (2017).

[25] Frangi, A., Guerrieri, A., Carminati, R. and Mendicino, G., “Parametric Resonance in Electrostatically Actuated Micromirrors,” IEEE Trans. Ind. Electron. 64(2), 1544–1551 (2017).